ISSN (Print) 1226-1750
ISSN (Online) 2233-6656
Journal of Magnetics 31(2), 145-152 (2026) https://doi.org/10.4283/JMAG.2026.31.2.145

Gradient-Compensated Layer-Decreasing Permanent-Magnet Array for Scalable Transverse Magnetic-Field Generation

Jusen Guo[1,2], Kang Qiu[2,3], Linchen Hu[1,2], Wei Ding[1], Jialiang Luo[2], Chenghong Zhang[2,3], Wei Wang[2], and Zhigao Sheng[2]*

[1]Institutes of Physical Science and Information Technology, Anhui University, Hefei 230601, China
[2]High Magnetic Field Laboratory, HFIPS, Chinese Academy of Sciences, Hefei 230031, China
[3]University of Science and Technology of China, Hefei 230026, China

(Received 21 October 2025, Received in final form 16 May 2026, Accepted 18 May 2026)

Large transverse magnetic fields are important in particle manipulation, material processing, and magnetically actuated systems. Conventional generation methods, however, often require high power consumption or complex structures to mitigate field inhomogeneity. Here, we propose a gradient-compensated, layer-decreasing permanent-magnet array assembled from small commercial magnets to improve transverse field homogeneity in a low-cost and scalable manner. The design suppresses edge-field growth while preserving central enhancement, thereby enlarging the usable region without additional energy consumption. Finite element simulations predict a usable region spanning 58 % of the array length under a comparative uniformity criterion of (B_{max}-B_{min})/B_{max} = 25 %. Experiments on a six-layer prototype show that the field non-uniformity along the measured central line decreases from 65 % for the single-layer configuration to 13 % for the six-layer configuration, while the central field increases to 0.068 T. The proposed configuration provides a practical passive magnetic-field platform for moderate-uniformity applications such as magnetic actuation and material assembly, and it offers a scalable basis for further optimization.

Keywords : transverse magnetic field, permanent magnets, gradient-compensated array, scalable magnet design

1. Introduction

Uniform magnetic fields (UMFs) are important in many scientific and industrial systems because field homogeneity directly affects process stability and controllability. In magnetic resonance techniques, very stringent field uniformity is required, whereas in engineering applications such as magnetic separation, anisotropic material alignment, and magnetic actuation, moderate field uniformity over an extended region can already be useful [1-6]. Different applications therefore involve different trade-offs among field quality, working volume, structural complexity, and cost. In this context, developing low-cost strategies for generating moderate-uniformity transverse fields is of considerable practical interest.

UMFs can be classified into three primary configurations according to field orientation: axial, longitudinal, and transverse. Axial UMFs exhibit homogeneity along the central axis of a solenoid and are commonly generated by precisely spaced coaxial coils with optimized current ratios, achieving very high uniformity in confined volumes. Longitudinal UMFs are often realized using Aubert arrays or Helmholtz coils [7]. Transverse UMFs can be generated by saddle coils or by pairs of parallel permanent magnets, and they are important in applications such as magnetic levitation and cross-field particle manipulation [8-10]. Compared with axial or longitudinal uniform fields, generating a large transverse UMF is generally more difficult and costly because the available symmetry is weaker and edge effects are more pronounced. Even when specially structured coils are used, large-volume transverse fields often require substantial power input, thermal management, active compensation, and precise alignment. These factors increase system complexity and cost and motivate the exploration of passive permanent-magnet alternatives.

Besides electromagnetic coils, permanent magnets can also generate UMFs within limited working regions when

*Corresponding author: Tel: 13395518022
Fax: 0551-65591270, e-mail: zhigaosheng@hmfl.ac.cn

combined with suitable array designs. Their main advantages are passive operation, compactness, and reduced thermal-management requirements. A representative example is the Aubert array, which creates a highly uniform longitudinal field within a confined volume and has been used in compact magnetic systems. However, permanent-magnet-based transverse-field generation remains less common. The main challenges are that increasing magnet size or quantity often strengthens spatial inhomogeneity, classical arrangements such as Halbach arrays are better suited to axial or longitudinal fields [11, 12], and transverse fields are particularly sensitive to edge effects [13]. In this context, arrays assembled from smaller commercial magnets are attractive because they reduce fabrication difficulty and provide greater freedom for structural tuning.

Zhang *et al.* achieved a rotating uniform magnetic field by precisely controlling both the spatial arrangement of individual magnets and their dipole orientations, demonstrating potential applications in magnetically driven robotic systems [14]. Other studies have explored adjustable dipole fields using bi-layer Halbach arrays composed of small permanent magnets to generate radially uniform magnetic fields for magnetically actuated and optical applications [15, 16].

Current research predominantly focuses on generating longitudinal magnetic fields within limited spatial domains. While Halbach arrays have proven effective for producing longitudinal fields, their performance remains constrained by relatively small coverage areas [17-19]. Iwashita *et al.* [20] used finite element analysis to design a permanent-magnet cavity capable of generating uniform magnetic fields for high-power laser applications. Although that design offers flexibility and cost-effectiveness, it requires wedge-shaped magnets with magnetization directions varying continuously from 0° to 180°, which exceeds the capability of most commercially available low-cost magnets and therefore necessitates custom manufacturing.

Alternative approaches include the work of Jin *et al.*, who mathematically optimized magnetic circuits using high-permeability materials to guide flux distribution between two large permanent magnets (420 × 360 mm), thereby achieving uniform longitudinal fields for food-processing applications. Cooley *et al.* [21] demonstrated a compact desktop MRI system using two opposing circular permanent magnets, each weighing 80 kg.

For transverse-field generation, McGinly *et al.* [22] successfully implemented uniform magnetic fields for MRI applications through finite element analysis of small NdFeB magnet blocks with varying dimensions and positions. However, the use of bulk NdFeB permanent magnets presents significant challenges, including complex sintering processes, high material costs, and difficult installation procedures, with individual poles weighing approximately 350 kg. These limitations highlight that current methods for generating transverse magnetic fields are still constrained by either excessive cost or structural complexity [20].

In summary, current methods for generating uniform magnetic fields over extended regions using permanent magnets face two major challenges:

(1) High cost of customized solutions;

(2) Excessive weight and high cost of large-scale implementations.

Developing a lightweight, low-cost, and customization-free method for constructing uniform magnetic fields over extended regions using permanent magnet arrays is therefore of considerable practical interest.

In this work, we propose a gradient-compensated, layer-decreasing configuration based on small permanent magnets. The main contribution of this study is an engineering array architecture that differentially regulates edge and central field growth to improve the homogeneity of a transverse field while reducing magnet consumption. Both simulation and experiment show consistent trends: under the comparative criterion $(B_{max}-B_{min})/B_{max} = 25\ \%$, the usable region reaches 58 % of the magnet length, the field non-uniformity decreases from 65 % in the single-layer configuration to 13 % in the six-layer configuration, and the central field reaches 0.068 T. These results indicate that the proposed configuration can serve as a low-cost, modular platform for moderate-uniformity transverse-field applications, while more demanding precision applications will require further optimization and full-field validation.

2. Design and Theoretical Modeling

For a uniformly magnetized permanent magnet, the magnetic field can be described through an equivalent bound-current representation. In this framework, the magnetization gives rise to surface current density on the magnet boundary, and the resulting field can be calculated from the Biot-Savart law [23]. Based on this representation, the spatial distribution of the magnetic field generated by a rectangular permanent magnet can be expressed as:

$$B_x = \frac{\mu_0}{4\pi} I \int_{-\frac{h}{2}}^{\frac{h}{2}} dz \int_{-\frac{b}{2}}^{\frac{b}{2}} (z_p - z) \left(\frac{1}{r_1^3} - \frac{1}{r_3^3} \right) dy \tag{1}$$

$$B_y = \frac{\mu_0}{4\pi} I \int_{-\frac{h}{2}}^{\frac{h}{2}} dz \int_{-\frac{b}{2}}^{\frac{b}{2}} (z_p - z)\left(\frac{1}{r_2^3} - \frac{1}{r_4^3}\right) dx \tag{2}$$

$$B_z = \frac{\mu_0}{4\pi} I \int_{-\frac{h}{2}}^{\frac{h}{2}} dz \left\{ \begin{aligned} &\int_{-\frac{b}{2}}^{\frac{b}{2}} \left(\frac{x_p + \frac{a}{2}}{r_3^3} - \frac{x_p - \frac{a}{2}}{r_1^3} \right) dy \\ &+ \int_{-\frac{a}{2}}^{\frac{a}{2}} \left(\frac{y_p - \frac{a}{2}}{r_2^3} - \frac{y_p + \frac{a}{2}}{r_4^3} \right) dx \end{aligned} \right\} \tag{3}$$

$$r_{1,3} = \left(x_p \pm \frac{a}{2}\right)^2 + \left(y_p - y\right)^2 + \left(z_p - z\right)^2 \tag{4}$$

$$r_{2,4} = \left(x_p - x\right)^2 + \left(y_p \pm \frac{b}{2}\right)^2 + \left(z_p - z\right)^2 \tag{5}$$

Here, B_x, B_y, and B_z represent the components of the magnetic field in the x, y, and z directions, respectively. *a*, *b*, and *h* represent the length, width, and height of the permanent magnet, respectively. In this study, the magnets are cubes, so all three geometric parameters are equal. The vacuum permeability is denoted by μ_0. Owing to the superposition principle of magnetic fields, for a magnet configuration consisting of N_1 magnets in the first layer, with m magnets reduced per layer and a total of *L* layers, the number of magnets in layer n is expressed as:

$$N_n - N_1 - m(n-1), n = 1,2,3\ldots L \tag{6}$$

Consequently, the magnetic field at point *P* is expressed as:

$$B_x(P) = \sum_{n=1}^{L} \sum_{i=1}^{N_n} B_x^{(n,i)}(x - x_n) \tag{7}$$

Based on the above analytical description, field superposition in multi-layer arrays can be interpreted physically, whereas FEM simulations are employed below for the quantitative evaluation of the proposed configurations.

3. Numerical Simulation

To compare the Equal-Stacked Array (ESA) and Gradient-Compensated Array (GCA), we performed FEM simulations for both configurations. For clarity, arrays with different layer counts are denoted as *x*LE, where *x* represents the number of layers. As shown in Fig. 1(a), the ESA contains 11 magnets in each layer and adopts a tightly stacked configuration with the magnetization oriented from left to right. To minimize the influence of pole reversal at the boundaries, the analysis region was defined as the air gap from the second to the second-to-last small magnet, corresponding to a rectangular region of 9 × 1 cm. Fig. 1(b) presents the magnetic-field distribution in this region for ESA configurations with one to six layers. In 1LE, the magnetic flux density is highest near the edges (±4.5 cm, 0.084 T) and decreases toward the center to 0.012 T. As the number of layers increases, the overall field strength rises nearly linearly across the region. The increment is 0.015 T/layer at the edges and 0.016 T/layer at the center, indicating nearly identical growth rates at both locations. Consequently, the field-distribution curves shift upward almost in parallel, and the relative gradient changes only slightly. In 6LE, the edge field reaches 0.161 T and the center field reaches 0.065 T, approximately four times the values in 1LE.

Although the ESA configuration exhibits clear layer-number dependence and an overall linear enhancement in field strength, it does not substantially improve uniformity. Because the edge and central fields grow at nearly identical rates, the gradient remains nearly unchanged. As a result, the usable region remains limited to 43 % of the

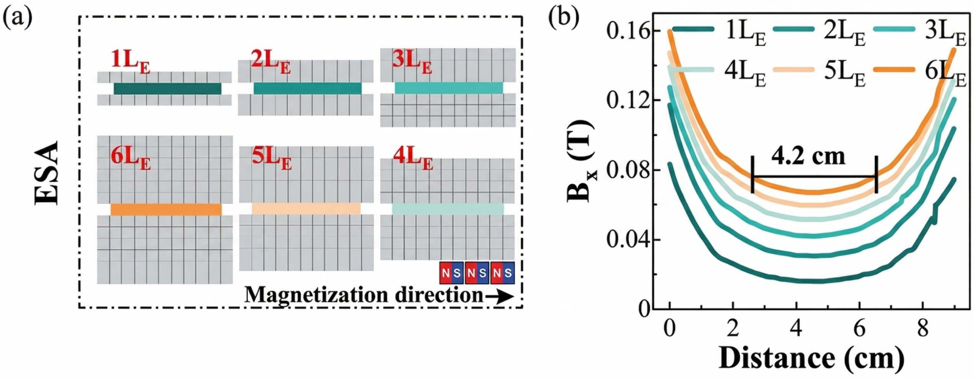

Fig. 1. (Color online) (a) Schematic diagram of the Equal-Stacked Array (ESA), with the magnetization direction indicated in the array; (b) Magnetic-field distribution at the configuration center.

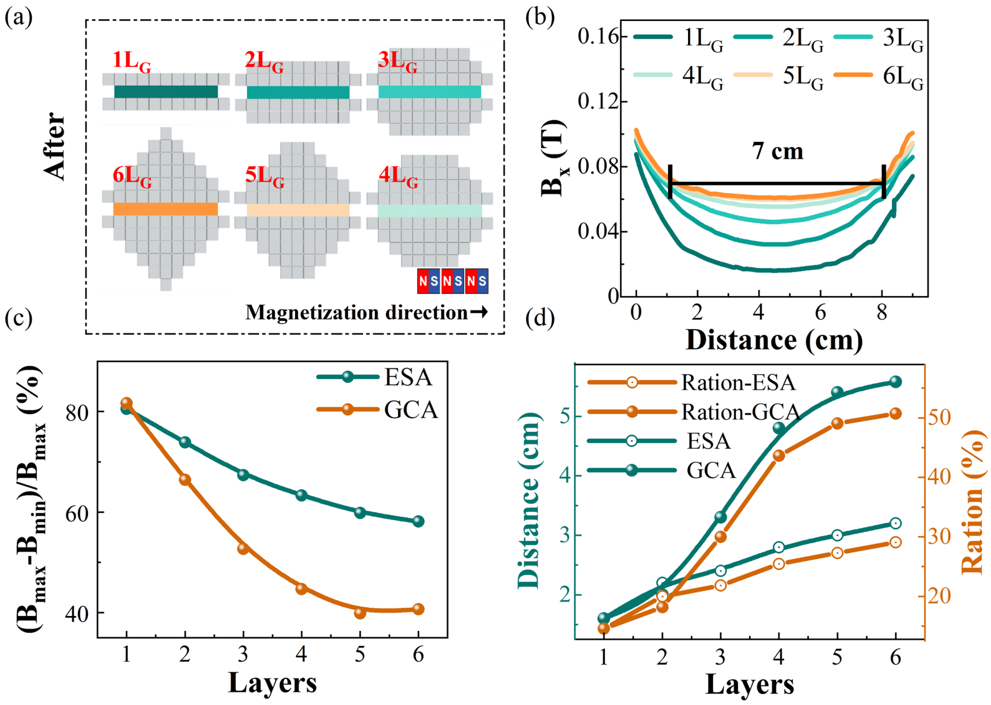

Fig. 2. (Color online) (a) Schematic diagram of the GCA, with the magnetization direction indicated in the array; (b) Magnetic-field distribution in the target region of GCA; (c) Uniformity comparison between two configurations; (d) Variation of usable distance and its proportion for both configurations.

total length at 6LE under the criterion $(B_{max}-B_{min})/B_{max}$ = 25 %. In this study, this threshold is used as a comparative engineering index for evaluating different configurations under the same framework [24, 25]. It should not be regarded as a universal requirement for precision magnetic systems, which generally demand much stricter uniformity.

To overcome this inherent limitation, we introduce a GCA configuration. Unlike the equal-stacked scheme, the GCA systematically reduces the number of magnets per layer, creating a built-in compensation mechanism that suppresses edge-field growth while maintaining central enhancement. This design uses fewer magnets in total, thereby achieving lower cost, and directly addresses the uniformity bottleneck observed in the ESA, enabling a significant expansion of the usable uniform region. Compared with Halbach-type or Aubert arrays, the present GCA trades absolute field quality for lower cost, simpler assembly, and the exclusive use of identical commercial magnets without custom fabrication.

Extending the spatial range of a usable transverse field remains challenging in practice. To address this issue, we developed the GCA model shown in Fig. 2(a). Arrays with different numbers of layers are denoted as *x*LG, where x is the layer count. Compared with the ESA, the GCA employs a symmetrically decreasing number of magnets along the stacking direction. A single-layer GCA exhibits the same initial field distribution as the ESA, as shown in Fig. 2(b). As the number of layers increases, however, the edge-field growth rate in the GCA is only 0.006 T/layer, whereas the central-field increase is 0.012 T/layer, close to that of the ESA. As a result, both configurations yield similar central fields (about 0.072 T), but the GCA suppresses edge enhancement more effectively. Fig. 2(c) shows that the uniformity index $(B_{max}-B_{min})/B_{max}$ decreases from 80 % to 40 % in the GCA, corresponding to a 40 % reduction, whereas the ESA shows only a 17 % reduction (80 % to 63 %). Under the selected 25 % criterion, the usable region of the GCA increases nonlinearly with layer count and approaches convergence at 5LG, whereas the ESA shows only slow linear growth. At convergence, the usable range reaches 58 % of the total length for the GCA, compared with 43 % for the ESA.

Clarifying the compensation mechanism constitutes a key difficulty due to the intricate interactions among different magnet layers. To address this, we quantitatively evaluated the contribution of each layer through numerical simulations (Figs. 3a and 3b). MagL*x* specifies the ordinal layer position (e.g., MagL3 denotes the third layer), not the total layer count. Each newly added layer is shortened by 1 cm on both ends relative to the one below, concent-

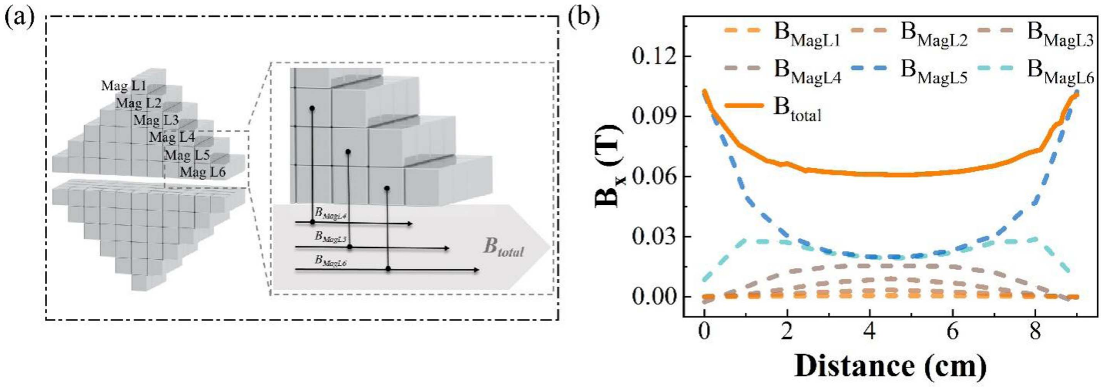

Fig. 3. (Color online) (a) Contribution of each magnet layer in the GCA configuration to the target region; (b) Numerical analysis of magnetic field compensation.

rating its magnetic enhancement closer to the central axis and thereby offsetting the attenuation caused by the underlying layer. In the present study, this layer-decreasing rule is used as a practical heuristic design derived from the compensation mechanism, rather than as a globally optimized arrangement.

In the ESA, each layer contains the same number of edge and central magnets. Because the magnetic field decays spatially, edge magnets predominantly reinforce the peripheral region, whereas central magnets enhance the center. Since both regions are strengthened simultaneously, the edge and center fields increase at comparable rates, resulting in only a limited reduction in the inherent gradient. In contrast, the GCA intentionally shortens the upper layers by removing edge magnets. This design exploits the natural field profile of each layer, which is stronger near the ends and weaker toward the center, so that the shortened upper layers are positioned slightly inward relative to the layers beneath them. As a result, the stronger fringe fields of the upper layers compensate for the decaying central field of the wider lower layers. For example, because MagL5 is shorter than MagL6, the

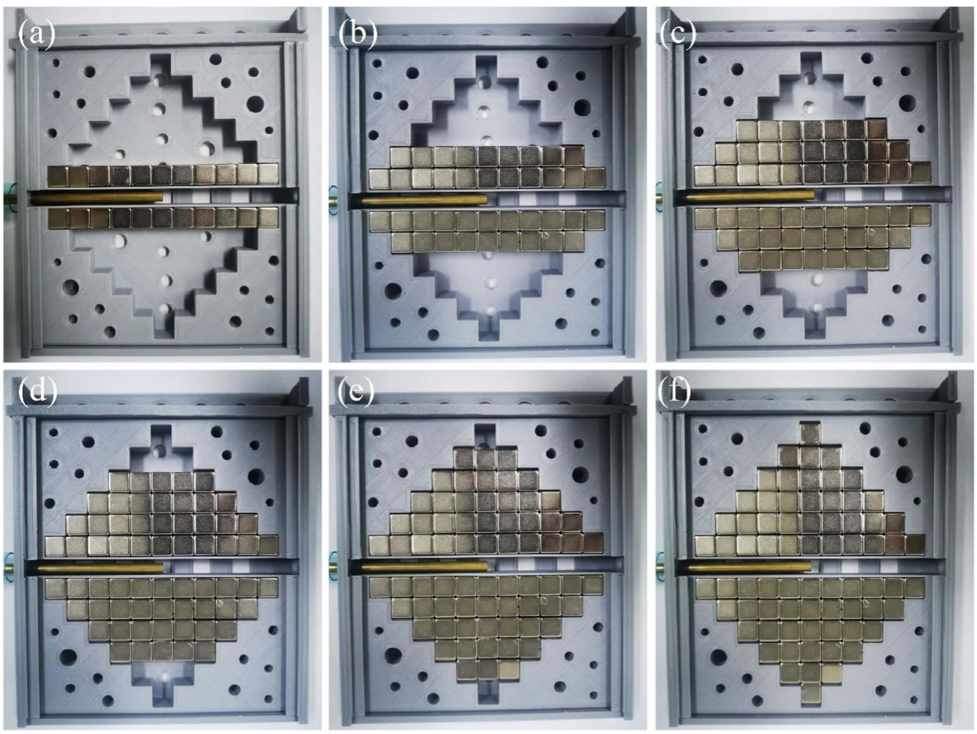

Fig. 4. (Color online) Physical prototypes of the multilayer gradient-compensated magnet configurations: (a) one layer; (b) two layers; (c) three layers; (d) four layers; (e) five layers; (f) six layers.

stronger field near the edge of MagL5 compensates for the attenuation of the field toward the center of MagL6. A similar compensation mechanism operates between the other layers. Overall, this gradient-decreasing design reduces the center-edge disparity, suppresses unwanted gradients, and improves field homogeneity with increasing layer number while also using fewer magnets, resulting in a more cost-effective and material-efficient configuration.

4. Experimental Validation

To validate the FEM trends, this study constructed a physical test platform based on the simulated parameters, as shown in Fig. 4. The experimental system employed commercial NdFeB permanent-magnet cubes (side length: 10.0 ± 0.2 mm, remanence: 1.45 T) as the basic units. Precision positioning fixtures were fabricated using high-resolution 3D printing technology with PETG material. The test specimens were fabricated according to the geometric parameters of the simulation model: the initial layer comprised 11 magnet units, and each successive layer contained two fewer units, forming a six-layer axisymmetric structure. The layers were arranged from top to bottom as the first through sixth layers of the magnet array, consistent with the simulation results shown in Fig. 3. Magnetic field measurements were carried out using a calibrated Hall-effect gaussmeter (TI/LZ-650) under standard laboratory conditions (25 ± 1 °C). A point-by-point scan was performed along the central axis of the magnet array (sampling interval: 10 mm, 11 measurement points), and each configuration was measured three times to obtain averaged values. Because the present experiment is limited to a one-dimensional line scan, the measured results are intended as proof-of-concept validation of the compensation strategy rather than a full two-dimensional uniformity characterization. Possible deviations may arise from probe positioning, fixture alignment tolerance, and remanence variation among commercial magnet units. The standard deviation across the three repeated measurements was estimated to be below 0.002 T at each point, dominated by the ±1 % full-scale accuracy of the Hall sensor, while the lateral positioning uncertainty along the central line was approximately ±0.5 mm, arising from the 3D-printed fixture tolerance and probe alignment.

To characterize the field response of the GCA prototype, we measured the magnetic flux density along the central line of the target region. Here, *x*L denotes the experimental configurations from one to six layers. As the number of magnet layers increases from 1L to 6L, the central magnetic field increases from 0.017 T to 0.068 T, corresponding to a 2.8-fold increase. The increment at the central position (x = 5.5 cm) is 0.010 T/layer, whereas the increment near the edge (x = 1 cm) is 0.0044 T/layer, indicating position-dependent field enhancement. The experimental trend in Fig. 5(a) is consistent with the FEM result in Fig. 2(b). FEM predicts a central increment of approximately 0.012 T/layer, close to the measured value of 0.010 T/layer, while the simulated edge increment (0.006 T/layer) is slightly higher than the measured value.

As shown in Fig. 5(b), the line-scan non-uniformity decreases from 65 % in the single-layer configuration to 13 % in the six-layer configuration. The most pronounced improvement occurs between 4L and 6L. Although the present measurements do not provide a full two-dimensional field map, the agreement between experiment and simulation supports the effectiveness of the proposed compensation strategy in improving central-line field homogeneity. To complement the $(B_{max}-B_{min})/B_{max}$ index, we also evaluated the root-mean-square deviation (RMSD) along the central line for the six-layer configuration. The

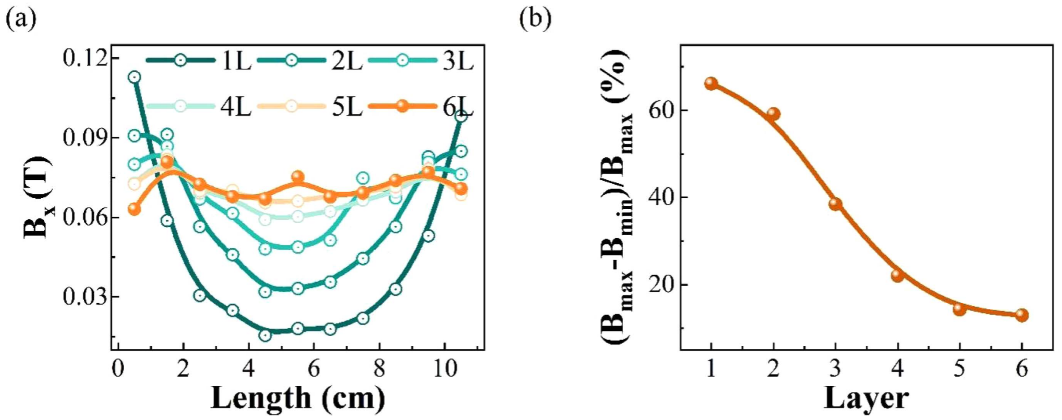

Fig. 5. (Color online) (a) Variation of central magnetic-field strength with layer count; (b) Evolution of magnetic field non-uniformity ($(B_{max}-B_{min})/B_{max}$) as a function of layer count.

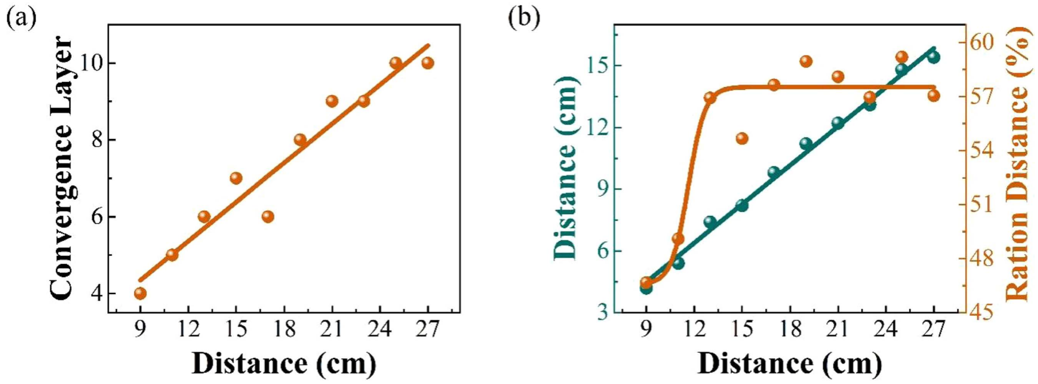

Fig. 6. (a) Relationship between convergence layer count and the number of magnets in the first layer; (b) Relationship between usable distance and its proportion under the uniformity threshold.

RMSD is approximately 0.005 T, corresponding to a relative deviation of about 8 % with respect to the mean field, which is consistent with the $(B_{max}-B_{min})/B_{max}$ = 13 % obtained from the same data set and provides an additional quantitative measure of the homogeneity improvement.

5. Parametric Scalability Analysis

To examine the scalability of the proposed heuristic design, we conducted a simulation-based parametric analysis. The system is considered to reach convergence when the inter-layer magnetic field variation ΔB in the central region is less than 0.001 T. Within the investigated range, increasing the first-layer length from 9 cm to 27 cm increases the convergence layer count from 4 to 10, showing an approximately linear trend. The usable distance under the selected 25 % criterion also increases with the number of magnets in the first layer. Meanwhile, the ratio of usable distance to first-layer length approaches 58 ± 2 % as N1 increases. These results indicate that the proposed array can be scaled in a predictable manner within the studied parameter range, although a broader optimization study is still needed.

6. Conclusion

This study presents a gradient-compensated, layer-decreasing permanent-magnet array for improving the homogeneity of a transverse magnetic field using identical small commercial magnets. By reducing edge contributions while preserving central enhancement, the configuration improves the usable region under a comparative engineering criterion and reduces magnet consumption relative to the equal-stacked array. Simulation and experimental line-scan measurements show consistent trends, with the usable region reaching 58 % of the array length under $(B_{max}-B_{min})/B_{max}$ = 25 %, the non-uniformity decreasing from 65 % to 13 %, and the central field reaching 0.068 T. These results support the proposed design as a low-cost, power-free, and modular platform for moderate-uniformity transverse-field applications such as magnetic actuation and material assembly. Further optimization and full-area field mapping, including two-dimensional RMS-based uniformity mapping over the entire target plane, will be required for more demanding precision applications.

Acknowledgement

We gratefully acknowledge financial support from the National Key R&D Program of China (Grant No. 2021YFA1600200, 2023YFA1607703), the National Natural Science Foundation of China (NSFC; Grant No. 12574136, 12404030), the Strategic Priority Research Program of Chinese Academy of Sciences (Grant No. XDB1300000). We thank the SM1 of the Steady High Magnetic field facility, CAS (https://cstr.cn/31125.02.SHMFF.SM1.MO) for the assistance on the experiment.

References

[1] J. Gao, Y. Zhen, Y. Zhang, and X. Wang, J. Magn. **29**, 380 (2024).
[2] P. Shin-Eui, J. Yeong-Jae, and B. Hyeon-Man, J. Magn. **30**, 40 (2025).
[3] F. Lin, G. Yang, C. Niu, Y. Wang, Z. Zhu, H. Luo, C. Dai, D. Mayerich, Y. Hu, J. Hu, X. Zhou, Z. Liu, Z. M. Wang, and J. Bao, Adv. Funct. Mater. **28**, 1805255 (2018).
[4] Y. Yuan, C. Han, L. Guo, X. Wu, and Y. Zhao, J. Mater. Chem. A **12**, 6165 (2024).

[5] K. Un Soo, H. Chang Su, L. Seung Han, K. Jun Ho, C. Sungwoo, and S. Donghoon, J. Magn. **29**, 284 (2024).
[6] K. Sung Hoon, J. Magn. **23**, 578 (2018).
[7] K. Menzel, J. A. Lindner, H. Soltner, and H. Nirschl, Sep. Purif. Technol. **134**, 220 (2014).
[8] H. Choi, K. Cha, J. Choi, S. Jeong, S. Jeon, G. Jang, J. O. Park, and S. Park, Sens. Actuators A Phys. **163**, 410 (2010).
[9] G. Xiao-fan, Y. Yong, and Z. Xiao-jing, Appl. Math. Mech. **25**, 297 (2004).
[10] Y. Jun, L. Decai, D. Nannan, and G. Ningning, J. Magn. **24**, 246 (2019).
[11] L. C. Barnsley, D. Carugo, J. Owen, and E. Stride, Physics in Medicine & Biology **60**, 8303 (2015).
[12] B. Fangfang, Z. Wenxiang, J. Jinghua, and X. Liang, J. Magn. **22**, 414 (2017).
[13] D. Sakellariou, C. Hugon, A. Guiga, G. Aubert, S. Cazaux, and P. Hardy, Magn. Reson. Chem. **48**, 903 (2010).
[14] W. Zhang, Y. Meng, and P. Huang, IEEE Trans. Magn. **44**, 2367 (2008).
[15] J. J. Abbott, E. Diller, and A. J. Petruska, Annu. Rev. Control Robot. Auton. Syst. **3**, 57 (2020).
[16] U. Bhunia, A. Agarwal, C. Das, C. Nandi, S. Mishra, P. Debnath, S. Pathak, S. V. Pratihast, A. Roy, J. Debnath, M. K. Dey, A. D. Gupta, and S. Som, Rev. Sci. Instrum. **96**, 043310 (2025).
[17] T.-O. Liang, Y. H. Koh, T. Qiu, E. Li, W. Yu, and S. Y. Huang, J. Magn. Reson. **345**, 107309 (2022).
[18] R. Ravaud, and G. Lemarquand, Progress in Electromagnetics Research-pier **98**, 207 (2009).
[19] C. Zhou, F. Lin, Y. Tang, Y. Liu, X. Luo, Y. Qi, S. Xu, Y. Qiu, H. Yan, X. Tong, A. Neogi, Z. Liu, X. Zhou, C. Wang, J. Bao, and Z. Wang, Mater. Today Phys. **31**, 100985 (2023).
[20] Y. Iwashita, Y. Kuriyama, and Y. Fuwa, IEEE Trans. Appl. Supercond. **34**, 1 (2024).
[21] C. Z. Cooley, J. P. Stockmann, T. Witzel, C. LaPierre, A. Mareyam, F. Jia, M. Zaitsev, Y. Wenhui, W. Zheng, P. Stang, G. Scott, E. Adalsteinsson, J. K. White, and L. L. Wald, J. Magn. Reson. **310**, 106625 (2020).
[22] J. V. M. McGinley, M. Ristic, and I. R. Young, J. Magn. Reson. **271**, 60 (2016).
[23] C. Luo, K. Zhang, J. Duan, and Y. Jing, J. Electr. Eng. Technol. **15**, 969 (2020).
[24] Y. Huang, L. Jiang, H. Lei, G. Gao, X. Deng, P. Wu, and J. Zhang, AIP Adv. **11**, 115125 (2021).
[25] X. Deng, Y. Huang, C. Wan, L. Jiang, G. Gao, Z. Huang, and J. Zhang, IEEE Trans. Plasma Sci. **50**, 1977 (2022).